Electronic Supplementary Information (ESI)

Helical fluxionality: numerical frustration drives concerted low-barrier screw motions of a tricopper cluster

Heechan Kim, Juhwan Shin, Seyong Kim, and Dongwhan Lee*

Department of Chemistry, Seoul National University, 1 Gwanak-ro, Gwanak-gu, Seoul 08826, Korea
*e-mail: dongwhan@snu.ac.kr

General Considerations. All reagents were purchased from commercial suppliers and used as received unless otherwise noted. The compounds 4-(*tert*-butyl)pyridine-2,6-dicarbaldehyde[1] and 4-methyl-7-(4,4,5,5-tetramethyl-1,3,2-dioxaborolan-2-yl)benzo[*c*][1,2,5]thiadiazole[2] were prepared according to literature procedures or their slight modifications. All air-sensitive manipulations were carried out under argon atmosphere in a glovebox or by standard Schlenk-line techniques.

Physical Measurements. ^{1}H NMR and ^{13}C NMR spectra were recorded on a 500 MHz Varian/Oxford As-500 spectrometer. Variable-temperature (VT) ^{1}H NMR spectra were recorded on a Varian Unity Inova 500 spectrometer or a Bruker Avance III 500 spectrometer. 2D ^{1}H–^{1}H Exchange Spectroscopy (EXSY) and Rotating-frame Nuclear Overhauser Effect Correlation Spectroscopy (ROESY) NMR spectra were recorded on a Varian Unity Inova 500 (UI500) spectrometer. DOSY NMR spectra were recorded on a 850 MHz Bruker Avance III HD spectrometer. Chemical shifts were referenced to internal standard of tetramethylsilane (as δ = 0.00 ppm). High-resolution electrospray ionization (ESI) mass spectra were obtained on a Thermo Scientific LTQ Orbitrap XL mass spectrometer. Coldspray ionization (CSI) mass spectra were collected on a JEOL JMS-T100CS mass spectrometer equipped with a CSI source, using the following conditions: needle voltage = 2.2 kV; orifice 1 current = 50–500 nA; orifice 1 voltage = 0–20 V; ring lens voltage = 10 V; ion source temperature = 278 K; spray temperature = 233 K. FT-IR spectra were recorded on a Shimadzu IRTracer-100 FT-IR Spectrophotometer. Elemental analysis was performed by a PerkinElmer 2400 Series II CHNS/O Analyzer. Electronic absorption spectra for Job plot analysis were recorded on an Agilent 8453 UV–vis spectrophotometer with ChemStation software.

2-Bromo-5-isopropoxypyridine (2). A 100 mL round-bottom flask was charged with 2-bromopropane (4.45 g, 36.2 mmol) and DMF (30 mL). To the solution was added 6-bromopyridin-3-ol (3.00 g, 17.2 mmol) and K_2CO_3 (4.28 g, 31.0 mmol). The reaction mixture was heated at reflux for 18 h. After cooling to r.t., the mixture was diluted with EtOAc (100 mL), and washed with brine (50 mL × 3). The organic layer was dried over anhyd $MgSO_4$, filtered, and concentrated under reduced pressure. With CH_2Cl_2 as an eluent, flash column chromatography on SiO_2 furnished **2** as a brown oil (3.32 g, 15.4 mmol, yield = 89%). ^{1}H NMR (500 MHz, $CDCl_3$, 298 K) δ 8.03 (d, J =

[1] L. M. Thierer, Q. Wang, S. H. Brooks, P. Cui, J. Qi, M. R. Gau, B. C. Manor, P. J. Carroll and N. C. Tomson, *Polyhedron*, 2021, **198**, 115044.
[2] T. Yamamoto, R. Murakami and M. Suginome, *J. Am. Chem. Soc.*, 2017, **139**, 2557–2560.

2.7 Hz, 1H), 7.35 (d, J = 8.7 Hz, 1H), 7.07 (dd, J = 8.7, 3.0 Hz, 1H), 4.54 (m, J = 6.0 Hz, 1H), 1.35 (d, J = 6.0 Hz, 6H). ^{13}C NMR (125 MHz, $CDCl_3$, 298 K) δ 153.79, 138.80, 131.70, 128.14, 126.00, 71.12, 21.76. FT-IR (ATR, cm^{-1}): 3058, 2978, 2933, 2500, 2064, 1900, 1573, 1560, 1462, 1449, 1376, 1334, 1267, 1224, 1178, 1131, 1109, 1088, 1010, 945, 907, 861, 825. HRMS (ESI) calcd. for $C_8H_{10}BrNO$ $[M + H]^+$ 239.9818, found 239.9821.

4-(5-Isopropoxypyridin-2-yl)-7-methylbenzo[*c*][1,2,5]thiadiazole (3). A 250 mL 3-neck round-bottom flask was charged with **2** (2.91 g, 13.9 mmol), 4-methyl-7-(4,4,5,5-tetramethyl-1,3,2-dioxaborolan-2-yl)benzo[*c*][1,2,5]thiadiazole (2.56 g, 9.27 mmol), $Pd(PPh_3)_4$ (0.541 g, 0.463 mmol), and K_2CO_3 (3.84 g, 27.8 mmol) under an Ar atmosphere. To the mixture was added degassed THF (50 mL) and H_2O (10 mL). The reaction was heated at reflux for 22 h. After cooling to r.t., volatile fractions were removed under reduced pressure, and the residual material was diluted with CH_2Cl_2 (50 mL) and H_2O (50 mL). The aqueous phase was extracted into CH_2Cl_2 (50 mL × 3). The combined organic layer was dried over anhyd $MgSO_4$, filtered, and concentrated under reduced pressure. Flash column chromatography on SiO_2 (hexane:EtOAc = 100:0 to 85:15, v/v) furnished **3** as a yellow solid (2.39 g, 8.38 mmol, yield = 90%). ^{1}H NMR (500 MHz, $CDCl_3$, 298 K) δ 8.57 (d, J = 8.8 Hz, 1H), 8.43 (d, J = 2.8 Hz, 1H), 8.26 (d, J = 7.2 Hz, 1H), 7.49 (d, J = 7.2 Hz, 1H), 7.34 (dd, J = 8.8, 2.9 Hz, 1H), 4.67 (m, J = 6.0 Hz, 1H), 2.78 (s, 3H), 1.41 (d, J = 6.1 Hz, 6H). ^{13}C NMR (125 MHz, $CDCl_3$, 298 K) δ 156.22, 153.49, 152.90, 146.60, 139.25, 131.37, 129.49, 128.60, 128.50, 124.89, 122.24, 70.69, 21.96, 18.09. FT-IR (ATR, cm^{-1}): 3017, 2976, 2921, 1586, 1565, 1551, 1497, 1467, 1397, 1383, 1338, 1297, 1288, 1258, 1217, 1197, 1176, 1136, 1110, 1069, 1017, 946, 888, 847, 830. HRMS (ESI) calcd. for $C_{28}H_{34}N_3O$ $[M + H]^+$ 286.1009, found 286.1010.

3-(5-Isopropoxypyridin-2-yl)-6-methylcyclohexa-3,5-diene-1,2-diamine (4). A 250 mL round-bottom flask was charged with **3** (2.39 g, 8.38 mmol), $CoCl_2{\cdot}6H_2O$ (400 mg, 1.68 mmol), and EtOH (100 mL). The solution was cooled to 0 ℃, and $NaBH_4$ (3.18 g, 83.8 mmol) was added slowly. The reaction mixture was heated at reflux under an Ar atmosphere for 4 h. After cooling to r.t., volatile fractions were removed under reduced pressure, and the residual material was diluted with CH_2Cl_2 (50 mL). The mixture was cooled to 0 ℃, and H_2O (50 mL) was added carefully to quench the remaining $NaBH_4$. The aqueous phase was extracted three times with CH_2Cl_2 (50 mL × 3). The combined organic extracts were dried over anhyd $MgSO_4$, filtered, and concentrated under reduced pressure. Flash column chromatography on SiO_2 (hexane:EtOAc = 10:0 to 3:7, v/v) furnished **4** as an orange solid (1.86 g, 7.22 mmol, yield = 86%). ^{1}H NMR (500 MHz, $CDCl_3$, 298 K) δ 8.28 (d, J = 2.8 Hz, 1H), 7.56 (d, J = 8.8 Hz, 1H), 7.25 (dd, J = 8.8, 2.9 Hz, 1H), 6.96 (d, J = 8.0 Hz, 1H), 6.65 (d, J = 8.0 Hz, 1H), 4.62–4.57 (m, 1H), 2.23 (s, 3H), 1.37 (d, J = 6.1 Hz, 6H). ^{13}C NMR (125 MHz, $CDCl_3$, 298 K) δ 152.12, 152.00, 136.65, 134.36, 133.73, 124.00, 123.06, 122.96, 122.12, 120.39, 119.39, 70.76, 21.97, 17.60. FT-IR (ATR, cm^{-1}): 3365, 2975, 2929, 2854, 1611, 1553, 1500, 1473, 1460, 1434, 1383, 1334, 1267, 1243, 1220, 1176, 1136, 1109, 1018, 948, 907, 887, 838. HRMS (ESI) calcd. for $C_{33}H_{37}N_4O$ $[M + H]^+$ 258.1601, found 258.1604.

2,2'-(4-(*tert*-Butyl)pyridine-2,6-diyl)bis(4-(5-isopropoxypyridin-2-yl)-7-methyl-1*H*-benzo[*d*]imidazole) (L). A 100 mL 2-neck round-bottom flask was charged with **4** (599 mg, 2.33 mmol) and 4-(*tert*-butyl)pyridine-2,6-dicarbaldehyde (203 mg, 1.06 mmol). A portion of anhydrous EtOH (20 mL) was added, and the mixture was stirred at 50 °C. To the solution was added aqueous solution (4 mL) of $Na_2S_2O_5$ (0.406 g, 2.12 mmol). The reaction mixture was heated at reflux under Ar atmosphere for 21 h. After cooling to r.t., H_2O (10 mL) was added. The precipitate was isolated by filtration, washed with H_2O (50 mL), and dried in vacuo. Recrystallization from hot EtOH (100 mL) furnished **L** as a pink solid (0.458 g, 0.687 mmol, yield = 65%). ^{1}H NMR (500 MHz, $CDCl_3$,

298 K) δ 12.75 (s, 2H), 8.53 (s, 2H), 8.20 (d, J = 2.8 Hz, 2H), 7.96 (d, J = 8.8 Hz, 2H), 7.70 (d, J = 7.7 Hz, 2H), 7.30 (dd, J = 8.8, 2.9 Hz, 2H), 7.19 (d, J = 7.7 Hz, 2H), 4.26 (m, J = 6.0 Hz, 2H), 2.85 (s, 6H), 1.20 (d, J = 6.0 Hz, 9H). ^{13}C NMR (125 MHz, $CDCl_3$, 298 K) δ 162.74, 152.55, 150.82, 149.17, 148.52, 144.99, 136.82, 132.50, 130.91, 124.52, 122.84, 119.86, 119.67, 119.53, 70.52, 35.57, 30.70, 21.86, 16.97. FT-IR (ATR, cm^{-1}): 3406, 2973, 1613, 1560, 1472, 1447, 1385, 1374, 1348, 1318, 1285, 1266, 1229, 1136, 1111, 951, 812. HRMS (ESI) calcd. for $C_{33}H_{37}N_4O$ $[M + H]^+$ 666.3551, found 666.3554.

$[Cu_3L_2](BF_4)_3$ (1). A mixture of **L** (227 mg, 0.341 mmol), $Cu(MeCN)_4(BF_4)$ (161 mg, 0.512 mmol), and CH_2Cl_2 (20 mL) was stirred at r.t. under Ar for 20 h. To the mixture was added Et_2O (50 mL) to induce precipitation of greenish brown solid, which was isolated by filtration to afford **1** (284 mg, 0.159 mmol, yield = 93%). Anal. Calcd. for $Cu_3C_{82}H_{86}B_3F_{12}N_{14}O_4$: C, 55.25; H, 4.86; N, 11.00. Found: C, 55.22; H, 4.68; N, 10.73.

X-ray Crystallographic Studies on 1. Single crystals of **1** were prepared by slow diffusion of Et_2O into a MeCN solution of this material. A brown crystal (approximate dimensions 0.389 × 0.245 × 0.197 mm^3) was placed onto a nylon loop with Paratone-N oil, and mounted on an XtaLAB AFC12 (RINC): Kappa dual home/near diffractometer. The data collection was carried out using Cu Kα radiation and the crystal was kept at T = 93 K. A total of 27227 reflections were measured ($6.274° \leq 2\theta \leq 158.844°$). The structure was solved with SHELXT[3] using direct methods, and refined with SHELXL[4] refinement package of OLEX2.[5] A total of 9070 unique reflections were used in all calculations. The final $R1$ was 0.0565 ($I \geq 2\sigma(I)$) and $wR2$ was 0.1597 (all data). CCDC 2178526 contains the supplementary crystallographic data for this structure.

[3] G. M. Sheldrick, *Acta Cryst.*, 2015, **A71**, 3–8.

[4] G. M. Sheldrick, 2015, **C71**, 3–8.

[5] O. V. Dolomanov, L. J. Bourhis, R. J. Gildea, J. A. K. Howard and H. Puschmann, *J. Appl. Cryst.* 2009, **42**, 339–341.

Determination of $\Delta G^{\ddagger}$ using VT 1D ^{1}H NMR spectroscopy.[6,7]

With an exchange between two equally populated sites, the NMR resonance (ν) can be expressed as coupled sets of Bloch equations, assuming that the Larmor frequencies of the two equally populated states are $+\delta$ and $-\delta$.

$$\nu = \gamma B_1 M_z \frac{k(2\delta)^2}{(\delta-\omega)^2(\delta+\omega)^2 + 4k^2\omega^2} \tag{1}$$

Here, γ is the magnetogyric ratio; B_1 is the field; M_z is z magnetization; k is the exchange rate; ω is the frequency. At the coalescence temperature T_c, the top of the lineshape is flat. Therefore, both the first and second derivatives with respect to the frequency (ω) have to be zero. The rate constant k_c at T_c is thus given by eq (2).

$$k_c = \frac{\delta}{\sqrt{2}} \tag{2}$$

Since δ is in radian per second, 2δ equals $2\pi\Delta\nu$, where $\Delta\nu$ is the difference of chemical shift between the two resonances at the low temperature limit. From the Eyring equation (eq (3)), where k_B is the Boltzmann constant, h is the Flanck constant, and R is the gas constant,

$$k_c = \frac{k_B T_c}{h} e^{-\frac{\Delta G^{\ddagger}}{RT_c}} \tag{3}$$

$\Delta G^{\ddagger}$ is expressed as eq (4).

$$\Delta G^{\ddagger} = (1.912 \times 10^{-2})(T_c)\left(9.972 + \log(\frac{T_c}{\Delta\nu})\right) \tag{4}$$

[6] F. P. Gasparro and N. H. Kolodny. *J. Chem. Educ.*, 1977, **54**, 258–261.
[7] H. Günther, in *NMR Spectroscopy*, Wiley-VCH, New York, 3rd edn, 2013, ch. 13.

Determination of $\Delta G^{\ddagger}$ using VT 2D ^{1}H–^{1}H EXSY NMR spectroscopy.[8,9]

For a thermoneutral equilibrium of A $\rightleftharpoons$ B, the rate equations are given as eqs (5) and (6). Here, ${M_z}^A(t)$ and ${M_z}^B(t)$ are the deviations (from the Boltzmann distribution) of the magnetic moments in the z-direction of the hydrogen nuclear spins of A and B conformers, respectively, at time t; k is the rate constant for the thermoneutral equilibrium of conformational exchange; $\frac{1}{T_1}$ is the rate constant for T_1 relaxation.

$$\frac{d{M_z}^A(t)}{dt} = -k{M_z}^A(t) + k{M_z}^B(t) - \frac{1}{T_1}{M_z}^A(t) \tag{5}$$

$$\frac{d{M_z}^B(t)}{dt} = -k{M_z}^B(t) + k{M_z}^A(t) - \frac{1}{T_1}{M_z}^B(t) \tag{6}$$

The matrix representation of eqs (5) and (6) is

$$\frac{d}{dt}\begin{pmatrix}{M_z}^A\\{M_z}^B\end{pmatrix} = \begin{pmatrix}-k-\frac{1}{T_1} & k\\ k & -k-\frac{1}{T_1}\end{pmatrix}\begin{pmatrix}{M_z}^A\\{M_z}^B\end{pmatrix} \tag{7}$$

After a diagonalization of the matrix, the solution of the differential equation at $t = \tau_{\mathrm{m}}$ is expressed as:

$$\begin{aligned}\begin{pmatrix}{M_z}^A(\tau_m)\\{M_z}^B(\tau_m)\end{pmatrix} &= \begin{pmatrix}\cosh k\tau_m \exp\{-(k+{T_1}^{-1})\tau_m\} & \sinh k\tau_m \exp\{-(k+{T_1}^{-1})\tau_m\}\\ \sinh k\tau_m \exp\{-(k+{T_1}^{-1})\tau_m\} & \cosh k\tau_m \exp\{-(k+{T_1}^{-1})\tau_m\}\end{pmatrix}\begin{pmatrix}{M_z}^A(0)\\{M_z}^B(0)\end{pmatrix}\\ &= \begin{pmatrix}a_{A\to A} & a_{B\to A}\\ a_{A\to B} & a_{B\to B}\end{pmatrix}\begin{pmatrix}{M_z}^A(0)\\{M_z}^B(0)\end{pmatrix}\end{aligned} \tag{8}$$

Therefore, the intensities of the diagonal (a_{diag}) and cross (a_{cross}) peaks are

$$a_{diag}(\tau_m) = a_{A\to A} = a_{B\to B} = \cosh k\tau_m \exp\{-(k+{T_1}^{-1})\tau_m\} \tag{9}$$

$$a_{cross}(\tau_m) = a_{A\to B} = a_{B\to A} = \sinh k\tau_m \exp\{-(k+{T_1}^{-1})\tau_m\} \tag{10}$$

The ratio of a_{cross} and a_{diag} is eq (11), which is independent of T_1.

$$\frac{a_{cross}(\tau_m)}{a_{diag}(\tau_m)} = \frac{\sinh k\tau_m}{\cosh k\tau_m} = \tanh k\tau_m \tag{11}$$

Using the relationship of

$$\tanh^{-1}\frac{a_{cross}(\tau_m)}{a_{diag}(\tau_m)} = k\tau_m \tag{12}$$

the rate constant k for the exchange reaction is obtained from the slope of the $(\tau_m, \tanh^{-1}\frac{a_{cross}(\tau_m)}{a_{diag}(\tau_m)})$ plot, as shown in **Fig. S16**.
The results are summarized in **Table S4** and **Table S5**.
Eyring analysis of these data provides the kinetic parameters $\Delta G^{\ddagger}$, $\Delta H^{\ddagger}$, and $\Delta S^{\ddagger}$ for the helical motion, as shown in **Fig. S17** and **Fig. S18**.

[8] J. Jeener, B. H. Meier, P. Bachmann and R. R. Ernst. *J. Chem. Phys.*, 1979, **71**, 4546–4553.
[9] P. W. Kuchel, B. T. Bulliman, B. E. Chapman and G. L. Mendz, *J. Magn. Reson.*, 1988, **76**, 136–142.

Table S1. Summary of X-ray crystallographic data for **1**.

	1
Chemical formula	$C_{43}H_{46}B_{1.5}Cu_{1.5}F_6N_8O_2$
Formula weight	932.40
Crystal system	monoclinic
Space group	$C2/c$
Color of crystal	Brown
a (Å)	29.3549(2)
b (Å)	14.38170(10)
c (Å)	21.2892(2)
α (°)	-
β (°)	106.3040(10)
γ (°)	-
Volume (Å^3)	8626.30(12)
Z	8
R_{int}	0.0227
Final R indices [$I > 2\sigma(I)$]	$R_1 = 0.0565$, $wR_2 = 0.1584$
Final R indices [all data]	$R_1 = 0.0581$, $wR_2 = 0.1597$
GOF	1.055

Table S2. Results of diffusion analysis on **1**.

Solvent	T (K)	η (10^{-4} Pa·s)	D (μm^2 s^{-1})	DOSY hydrodynamic radius[a] (Å)
THF-d_8	268	6.37[b]	482	6.40
	278	5.63[b]	590	6.13
	288	5.03[b]	690	6.08
	298	4.52[b]	728	6.62
$CDCl_3$	298	5.76[c]	845	4.77

[a] The hydrodynamic radius was estimated by the Stokes–Einstein equation: $D = kBT/6\pi\eta r$
[b] The temperature-specific viscosity η (in P) of THF was estimated by using the equation[10]: $\log \eta = -3.670 + 395/T$
[c] The viscosity of $CHCl_3$ at $T = 298$ K[11]

[10] D. J. Metz and A. Glines, *J. Phys. Chem.*, 1967, **71**, 1158.
[11] R. A. Clará, A. C. G. Marigliano, D. Morales, and H. N. Sólimo, *J. Chem. Eng. Data*, 2010, **55**, 5862–5867.

Table S3. Parameters obtained from VT 1D NMR spectroscopy in various solvents.

	T_c (K)	$\Delta\nu$ (Hz)	$\Delta G^{\ddagger}$ (kcal mol^{-1})
THF-d_8	273	130	12.9
acetone-d_6	228	200	10.5

Table S4. Kinetic parameters for the helical motion of **1** determined by VT 2D ^{1}H–^{1}H EXSY NMR spectroscopy in $CDCl_3$.

T [K]	k [s^{-1}]	ln k	ln (k/T)
313	33.89	3.523	–2.223
308	25.02	3.220	–2.510
303	18.57	2.922	–2.792
298	13.46	2.600	–3.097

Table S5. Kinetic parameters for the helical motion of **1** determined by VT 2D ^{1}H–^{1}H EXSY NMR spectroscopy in CD_2Cl_2.

T [K]	k [s^{-1}]	ln k	ln (k/T)
273	15.71	2.754	–2.855
268	6.465	1.866	–3.725
263	3.952	1.374	–4.198
253	1.017	0.017	–5.516

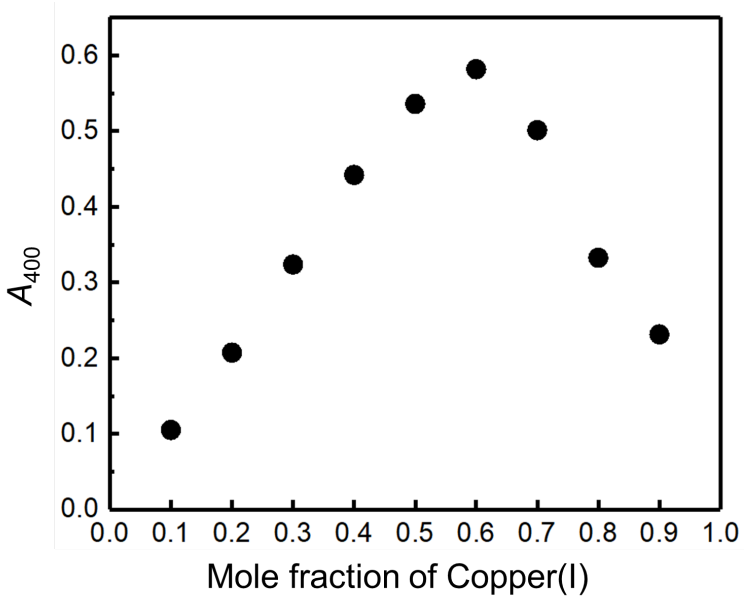

Fig. S1. Job plot analysis of the binding between $[Cu(MeCN)_4](BF_4)$ and **L** in THF (T = 298 K), plotted as absorbance at λ = 400 nm vs mole fraction of copper(I) ion.

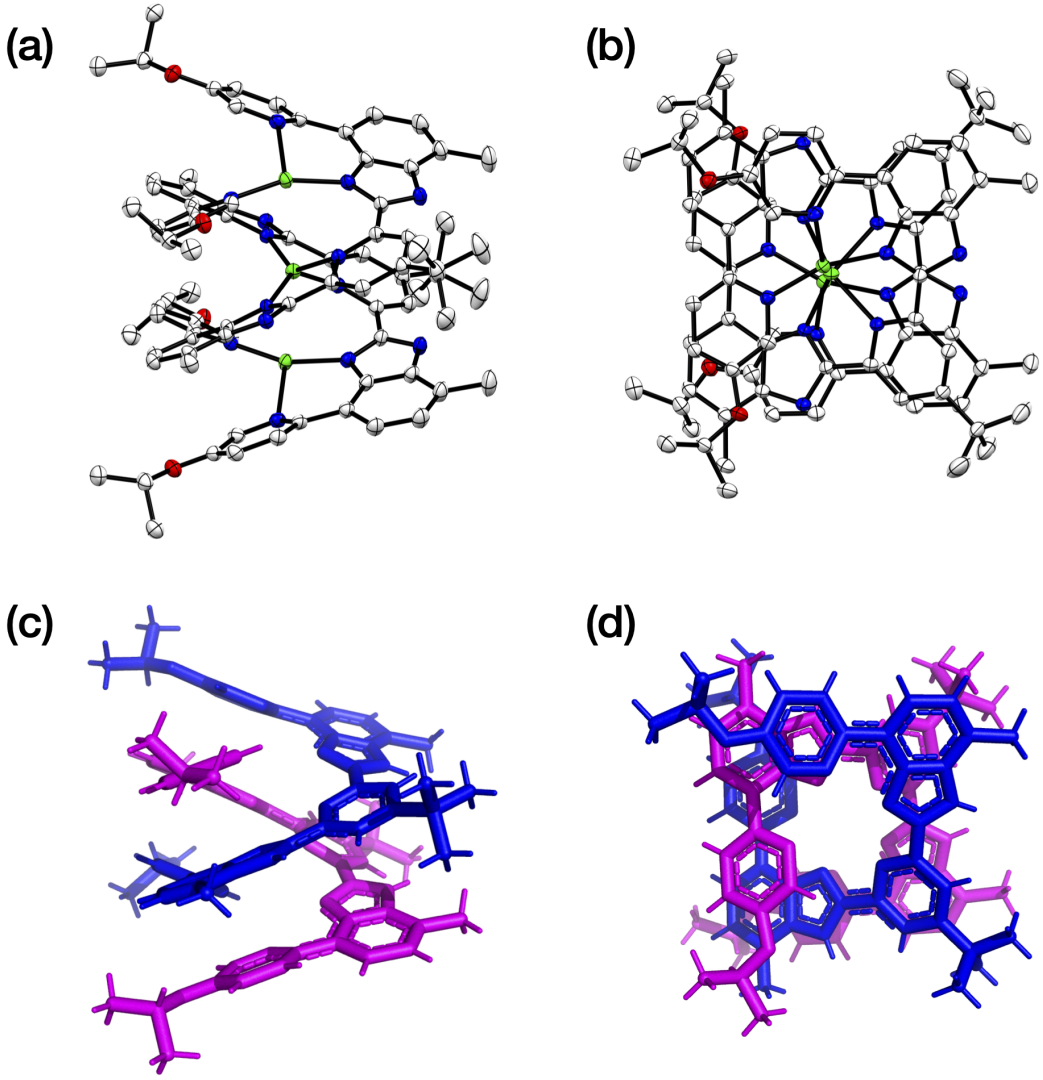

Fig. S2. X-ray structure of the cation of **1** as ORTEP diagrams with thermal ellipsoids at the 50% probability level (Cu is green, N is blue, and O is red): (a) side view; (b) top view. The hydrogen atoms were omitted for clarity. In (c) and (d) are capped-stick representations of individual ligand strands color-coded (blue and magenta) and metal atoms omitted to visualize the double-helical topology better.

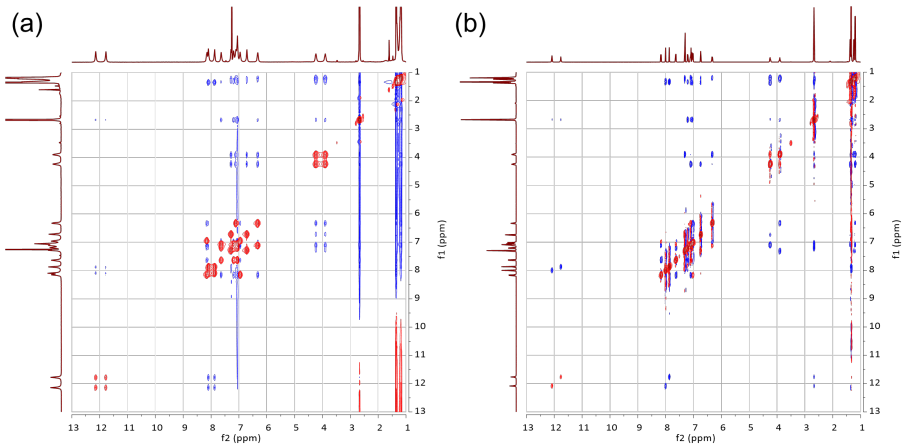

Fig. S3. 2D-ROESY NMR spectrum of **1** in $CDCl_3$ with t_m = 500 ms at (a) T = 298 K, and (b) T = 233 K; the corresponding 1D spectrum is shown along the ordinate. Blue (positive) signals are ROE resonances; red (negative) signals are exchange resonances.

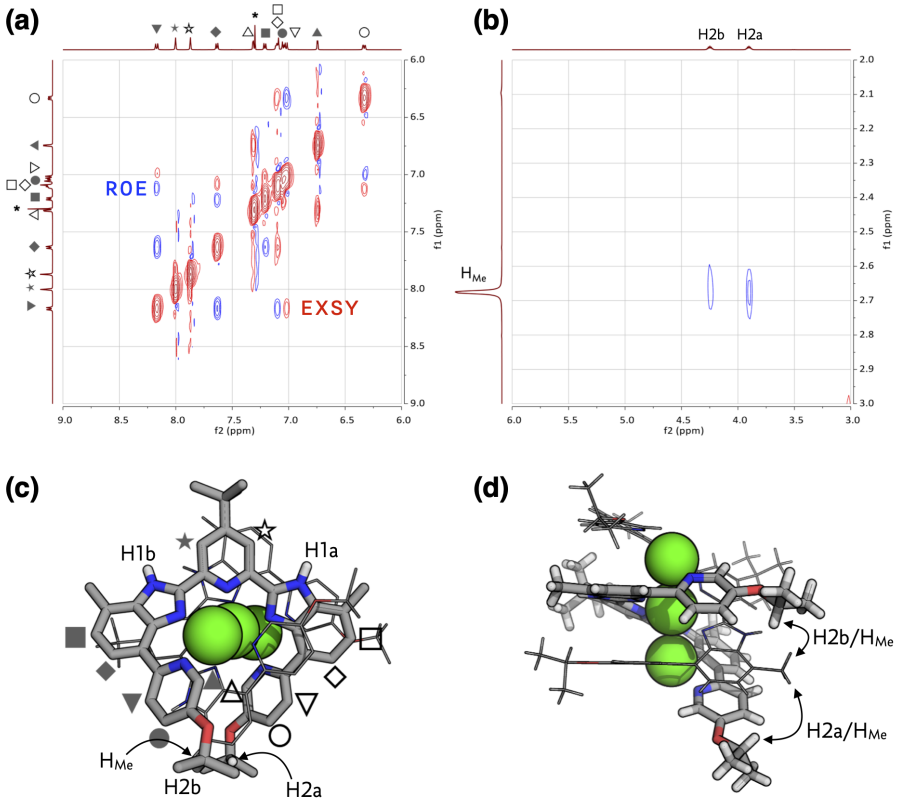

Fig. S4. 2D-ROESY NMR spectrum ($CDCl_3$, T = 233 K) of **1** in the (a) aromatic, and (b) aliphatic regions, along with (c) proton labeling scheme. Blue (positive) signals are ROE resonances; red (negative) signals are exchange resonances. (d) Through-space correlations between H_{Me} and H2a/H2b.

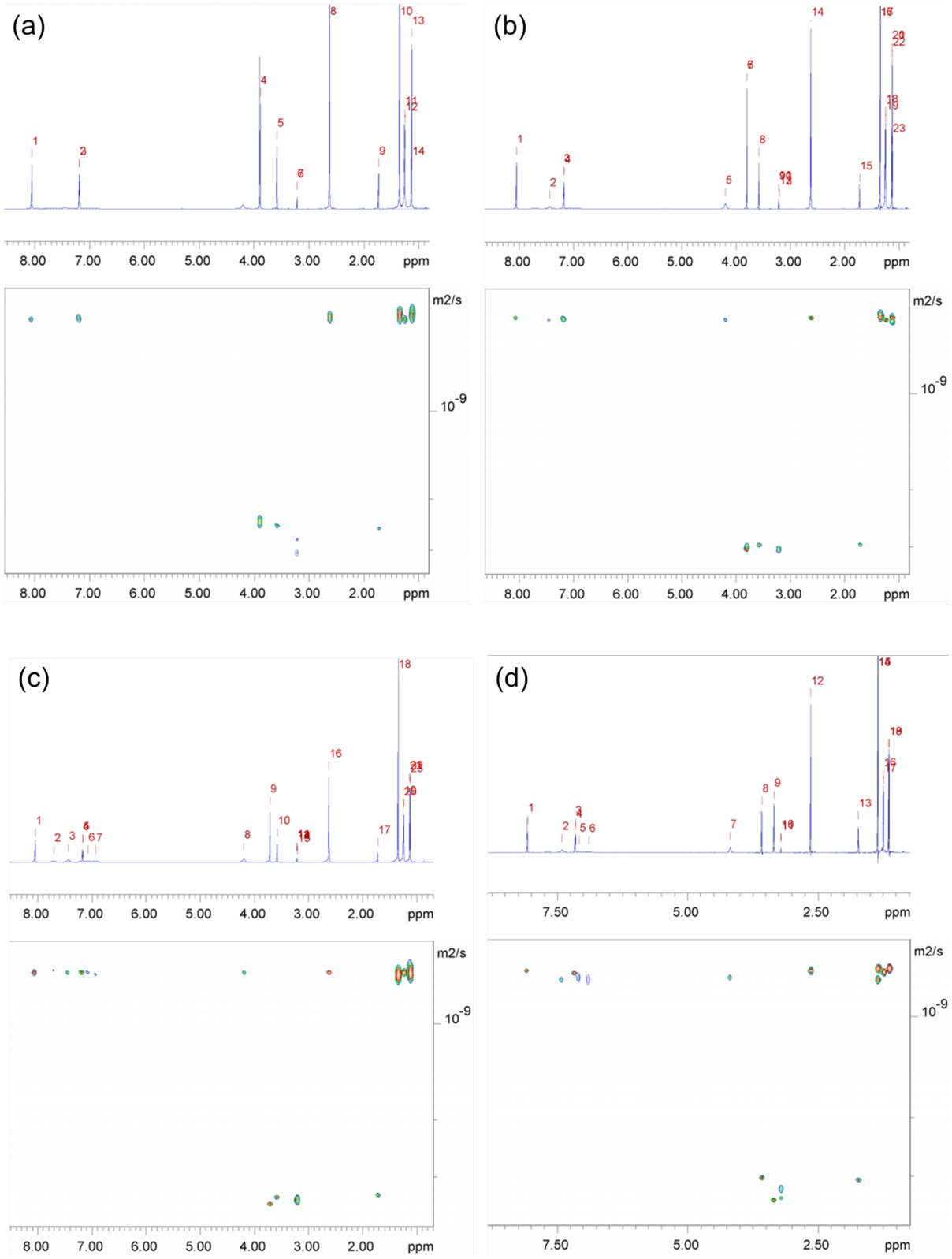

Fig. S5. ^{1}H DOSY NMR spectra of **1** in THF-d_8 at different temperatures of (a) 268 K, (b) 278 K, (c) 288 K and (d) 298 K.

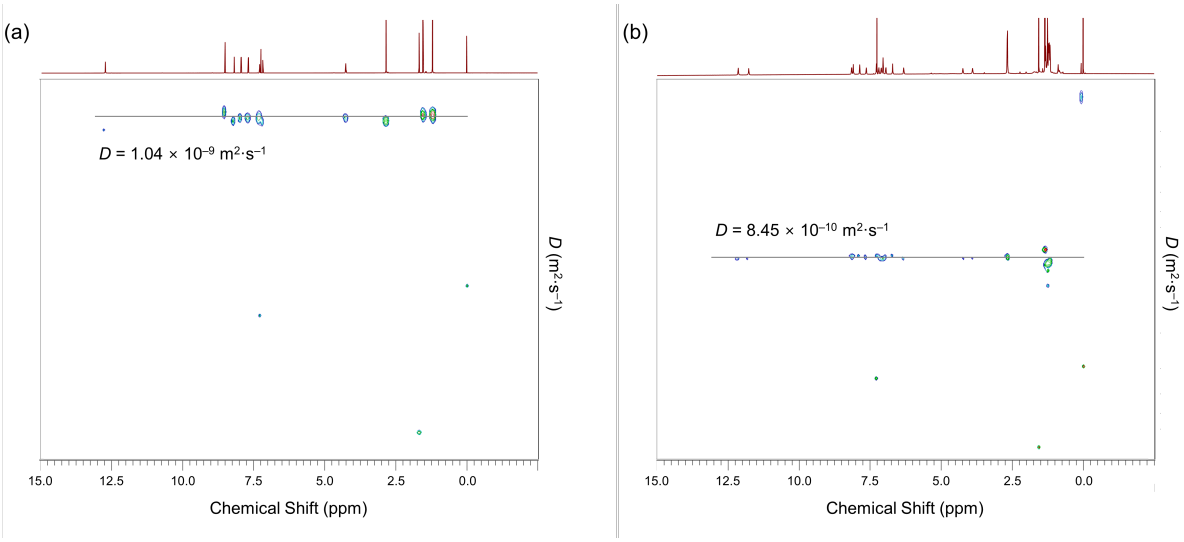

Fig. S6. ^{1}H DOSY NMR spectrum of (a) **L** and (b) **1** in $CDCl_3$ (T = 298 K).

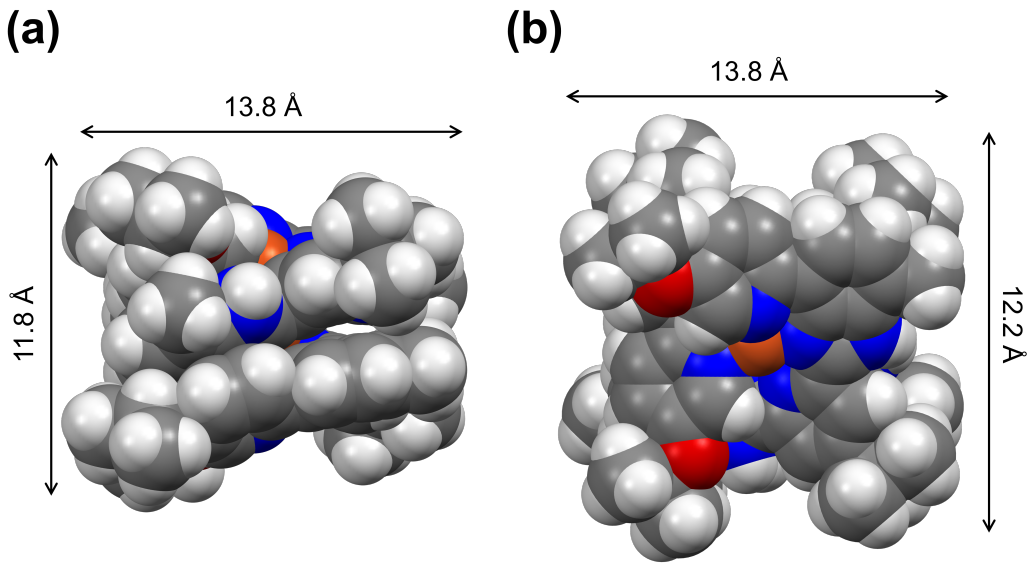

Fig. S7. (a) Side-on, and (b) face-on views of space-filling representations of the crystallographically determined three-dimensional structure of **1** cation.

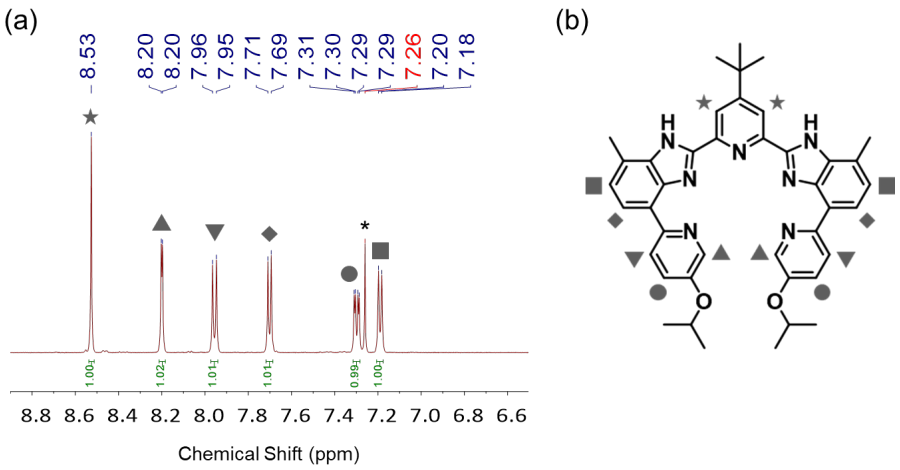

Fig. S8. (a) Partial ^{1}H NMR spectrum of **L** in $CDCl_3$ (T = 298 K) showing the aromatic region. The residual solvent is designated with an asterisk. (b) Chemical structure of **L** with the aromatic protons labelled.

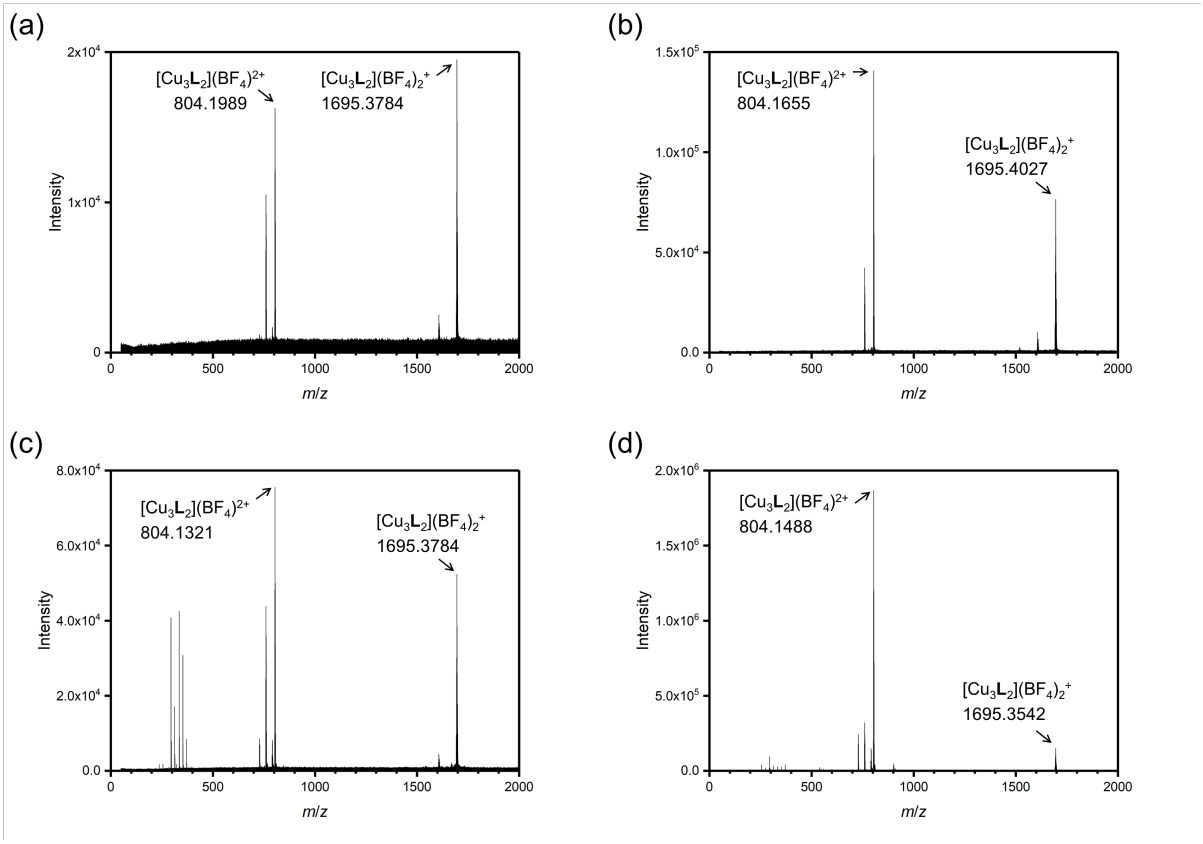

Fig. S9. CSI-MS spectra of **1** in (a) $CHCl_3$, (b) CH_2Cl_2, (c) THF, and (d) acetone at T = 233 K.

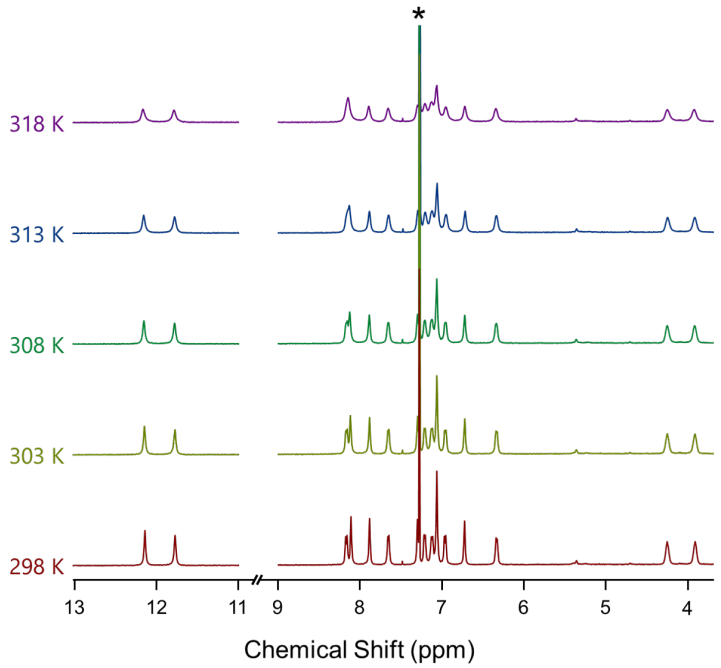

Fig. S10. Temperature-dependent (T = 298–398 K) changes in the ^{1}H NMR spectra of **1** in $CDCl_3$. The residual solvent is designated with an asterisk.

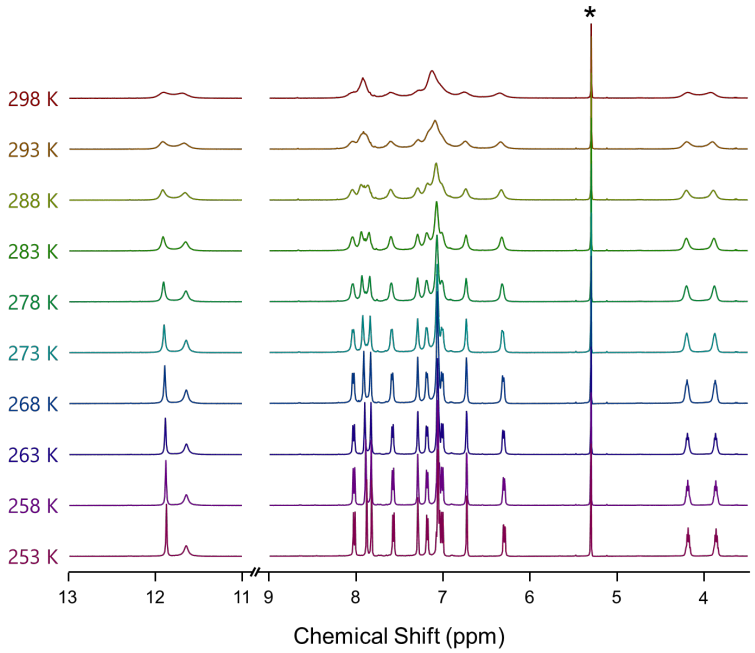

Fig. S11. Temperature-dependent (T = 253–298 K) changes in the ^{1}H NMR spectra of **1** in CD_2Cl_2. The residual solvent is designated with an asterisk.

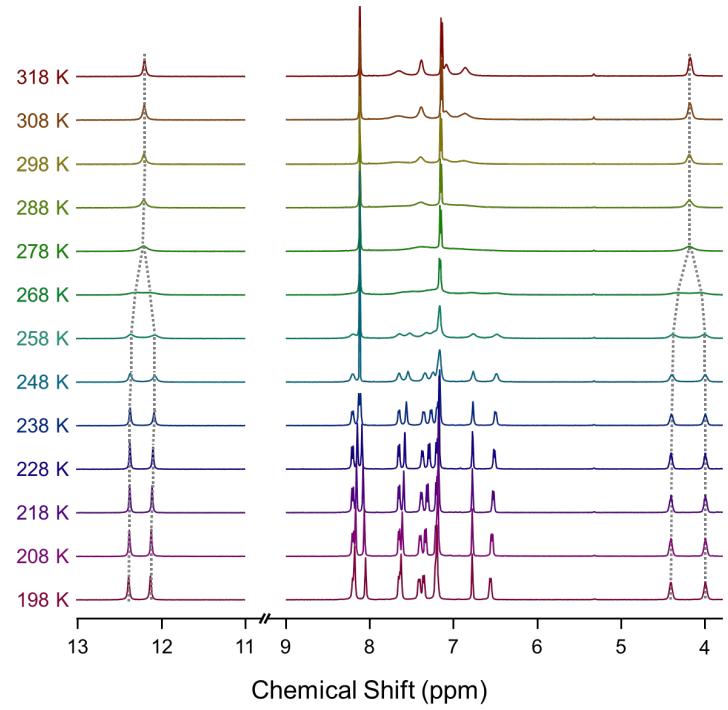

Fig. S12. Temperature-dependent (T = 198–318 K) changes in the ^{1}H NMR spectra of **1** in THF-d_8.

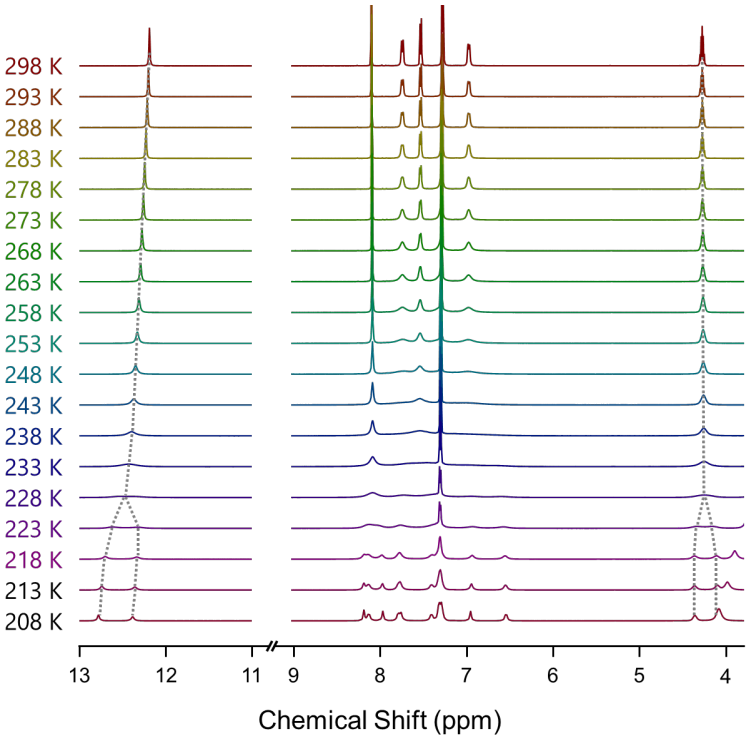

Fig. S13. Temperature-dependent (T = 208–298 K) changes in the ^{1}H NMR spectra of **1** in acetone-d_6.

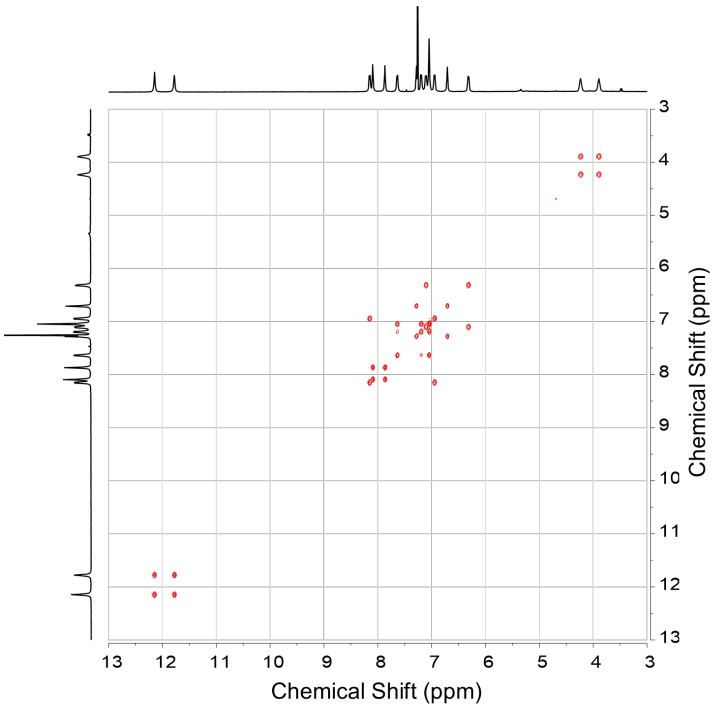

Fig. S14. Representative 2D ^{1}H–^{1}H EXSY NMR spectrum of **1** in $CDCl_3$ with t_m = 100 ms (T = 298 K).

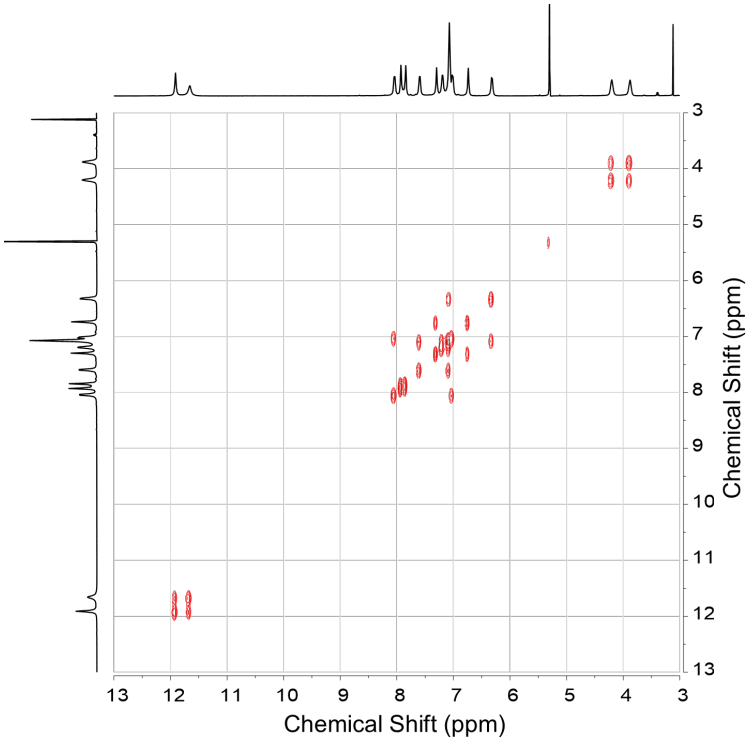

Fig. S15. Representative 2D ^{1}H–^{1}H EXSY NMR spectrum of **1** in CD_2Cl_2 with t_m = 50 ms (T = 273 K).

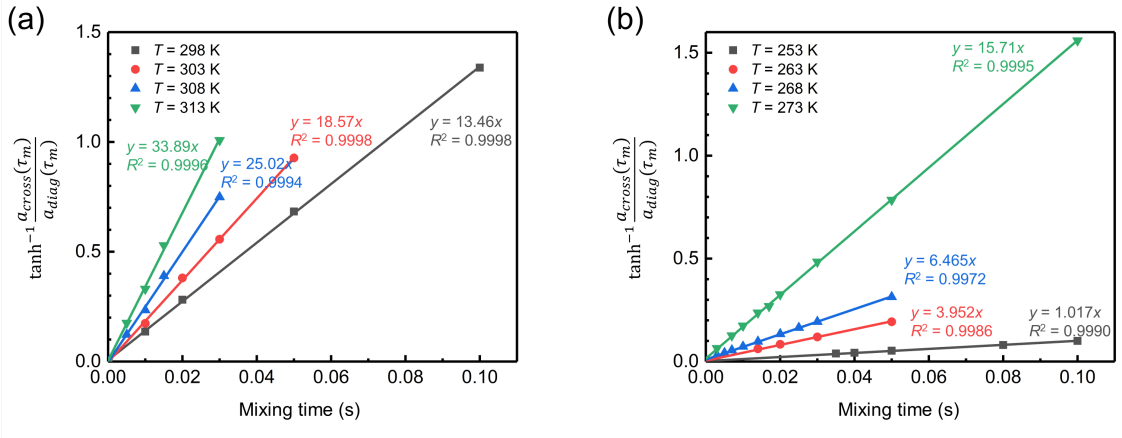

Fig. S16. Plots of mixing time vs $\tanh^{-1}\frac{a_{cross}(\tau_m)}{a_{diag}(\tau_m)}$ obtained at various temperatures in (a) $CDCl_3$, and (b) CD_2Cl_2.

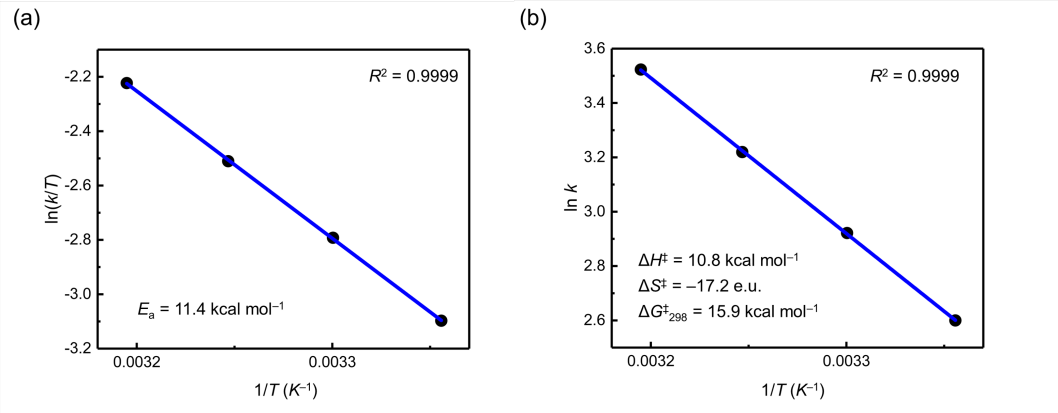

Fig. S17. (a) Arrhenius, and (b) Eyring plots constructed using the data in **Table S4** for the helical motions of **1** in $CDCl_3$.

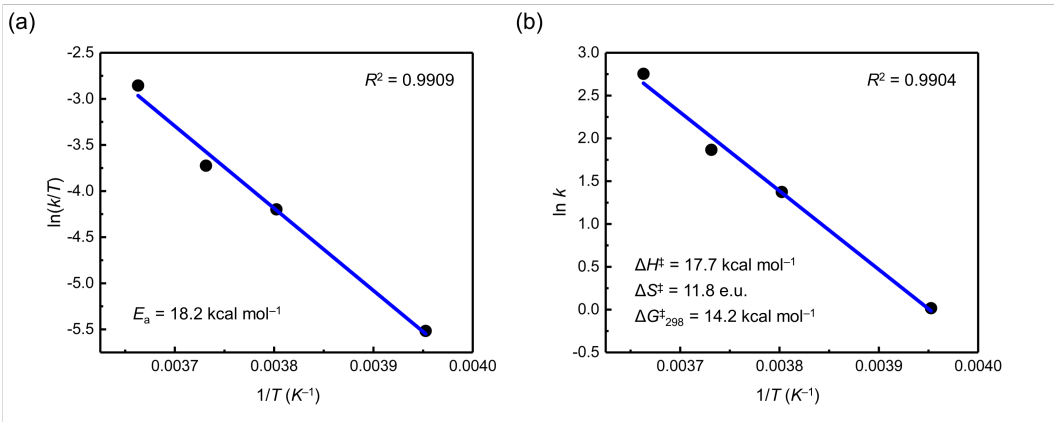

Fig. S18. (a) Arrhenius, and (b) Eyring plots constructed using the data in **Table S5** for the helical motions of **1** in CD_2Cl_2.

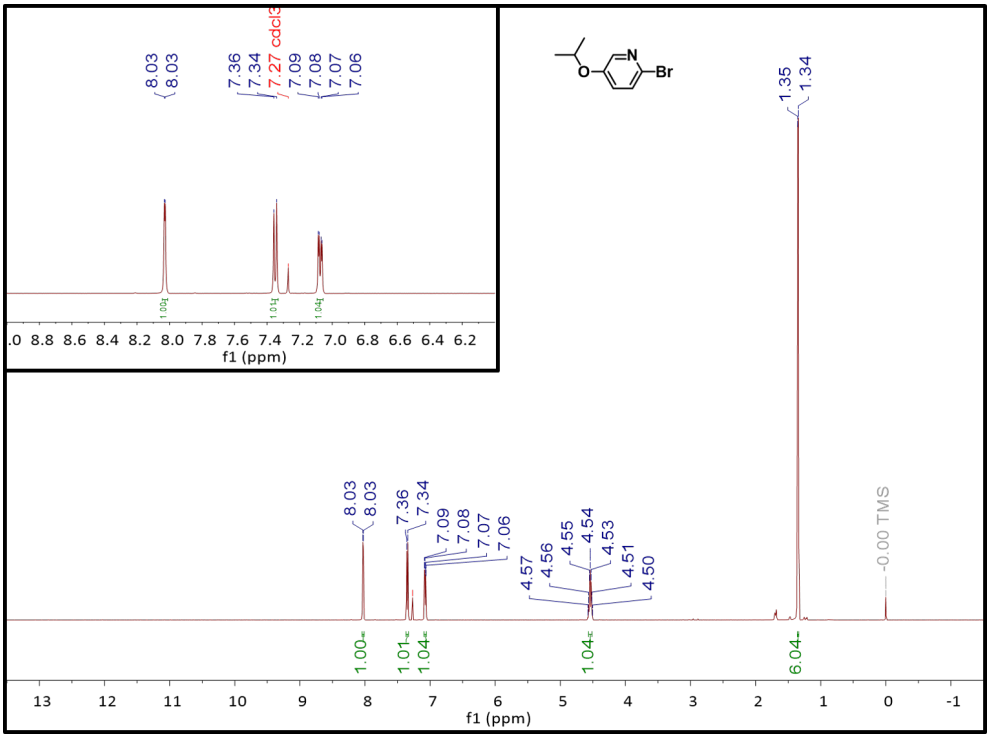

Fig. S19. ^{1}H NMR (500 MHz) spectrum of **2** in $CDCl_3$ (T = 298 K).

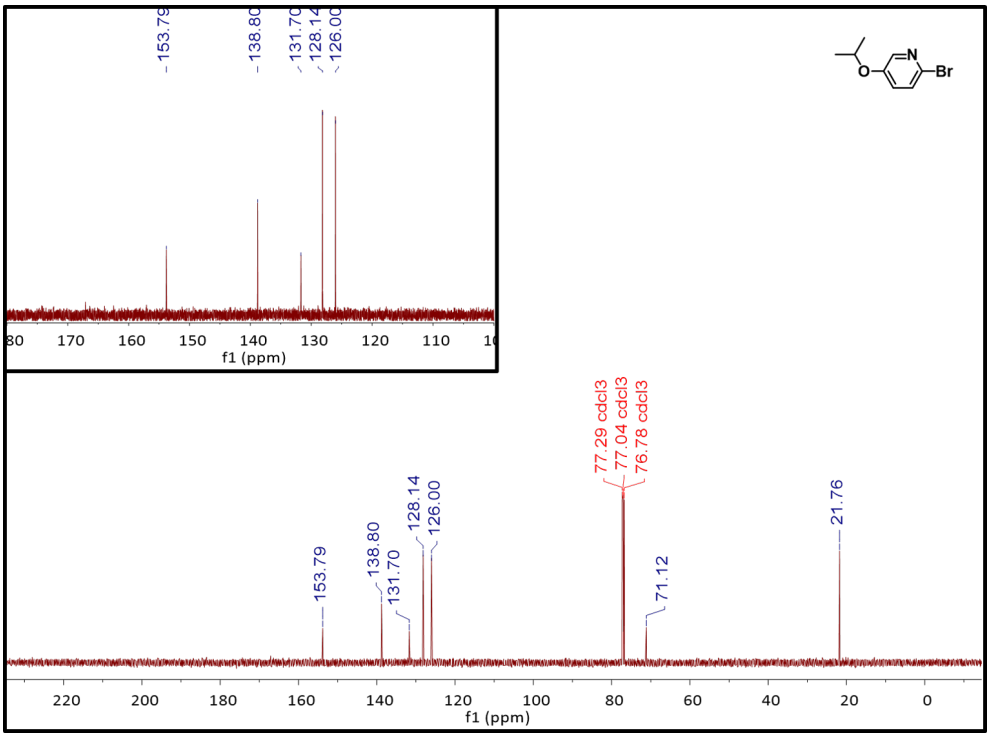

Fig. S20. ^{13}C NMR (125 MHz) spectrum of **2** in $CDCl_3$ (T = 298 K).

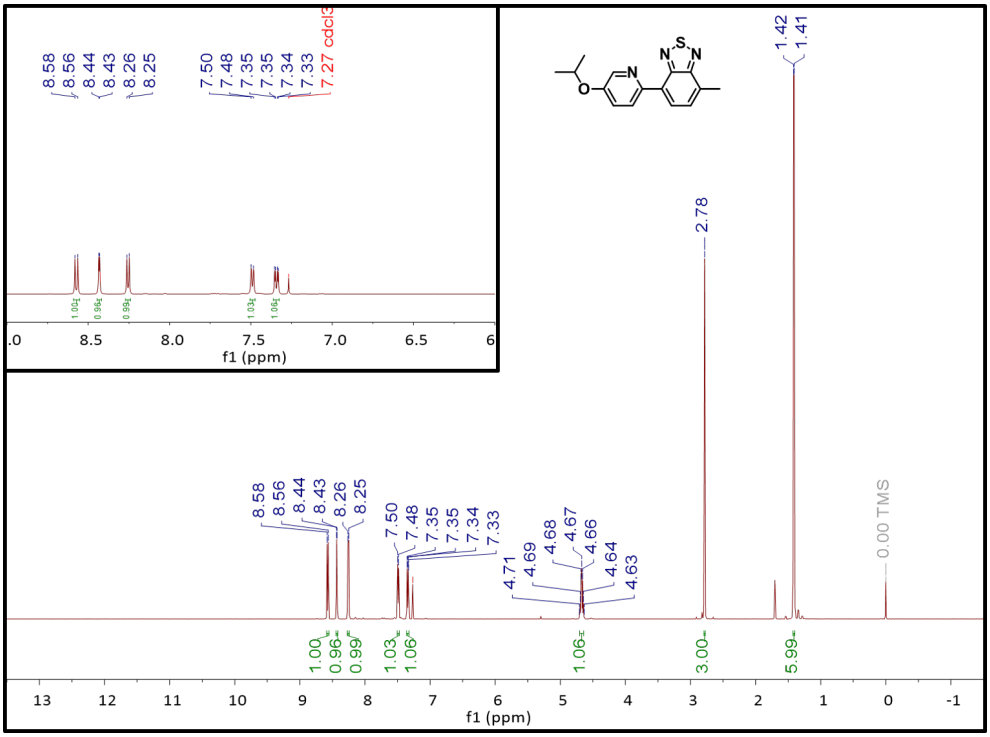

Fig. S21. ^{1}H NMR (500 MHz) spectrum of **3** in $CDCl_3$ (T = 298 K).

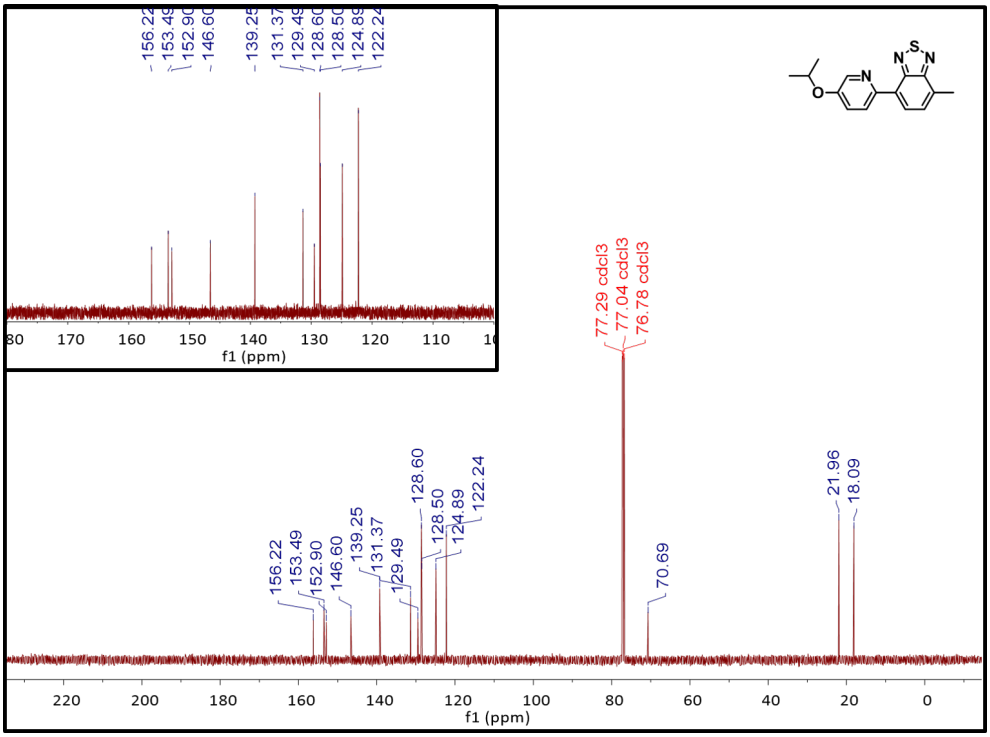

Fig. S22. ^{13}C NMR (125 MHz) spectrum of **3** in $CDCl_3$ (T = 298 K).

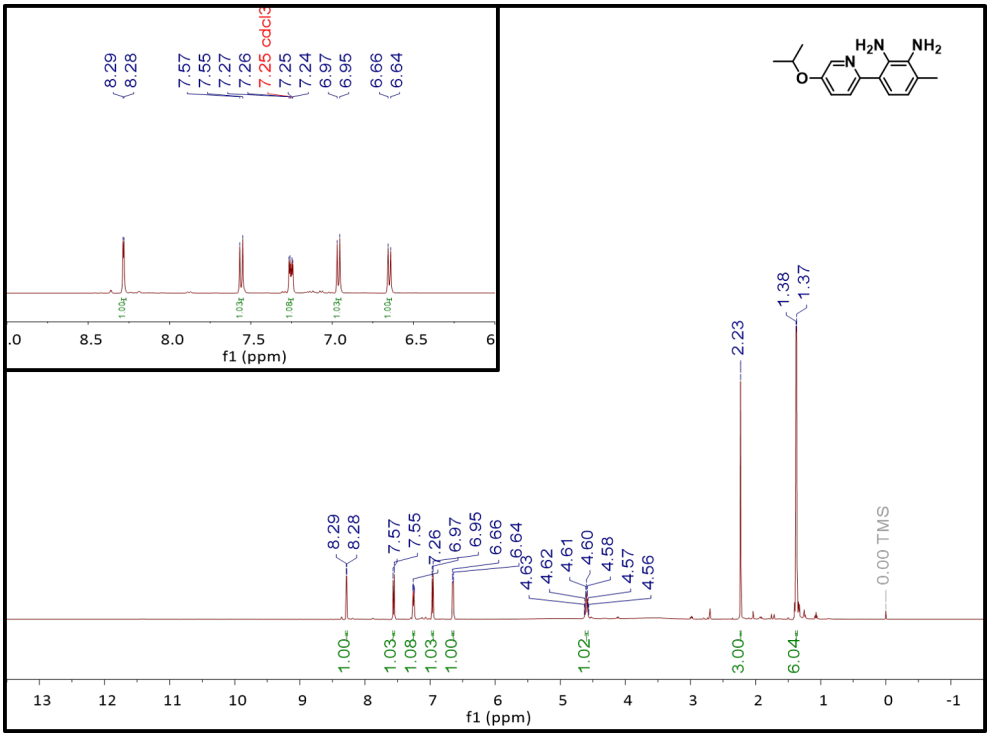

Fig. S23. ^{1}H NMR (500 MHz) spectrum of **4** in $CDCl_3$ (T = 298 K).

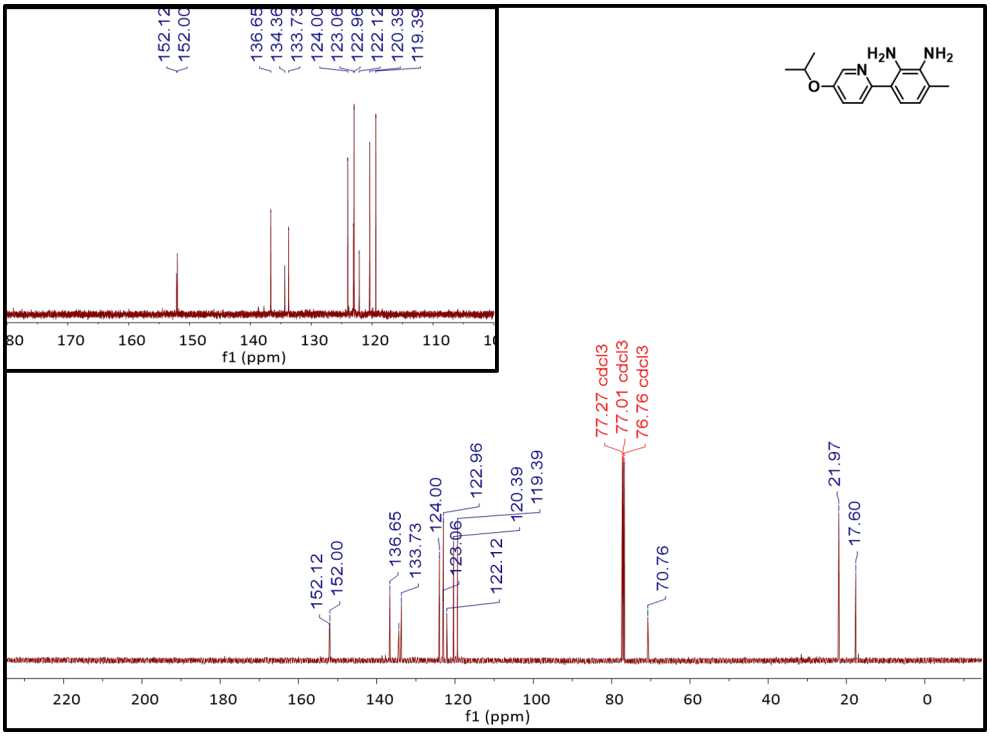

Fig. S24. ^{13}C NMR (125 MHz) spectrum of **4** in $CDCl_3$ (T = 298 K).

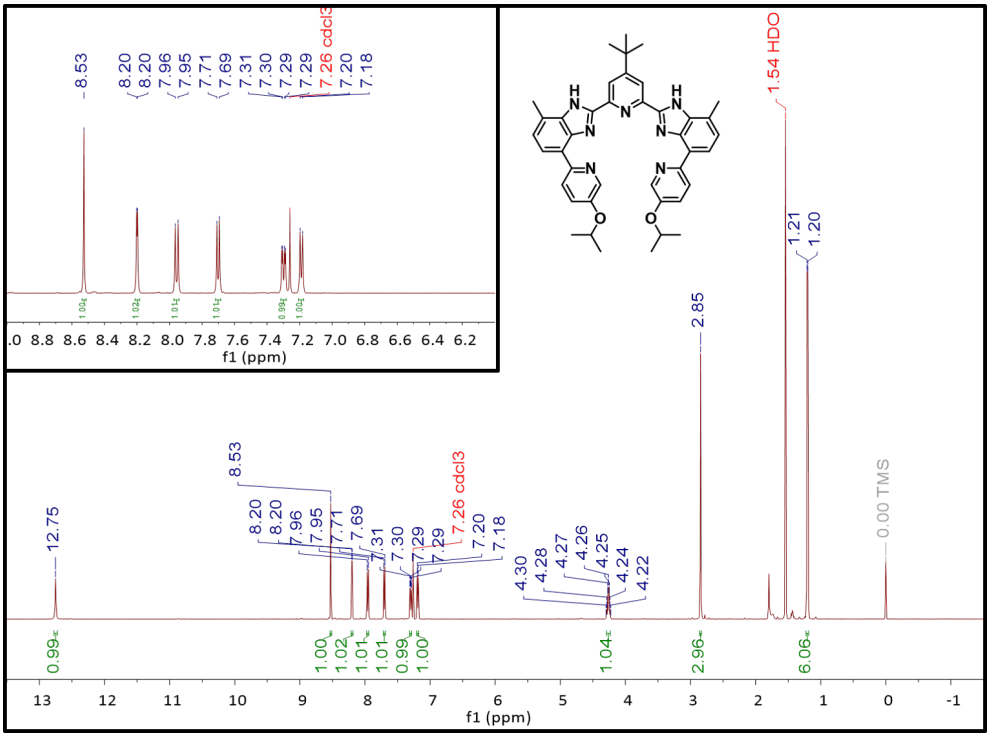

Fig. S25. ^{1}H NMR (500 MHz) spectrum of **L** in $CDCl_3$ (T = 298 K).

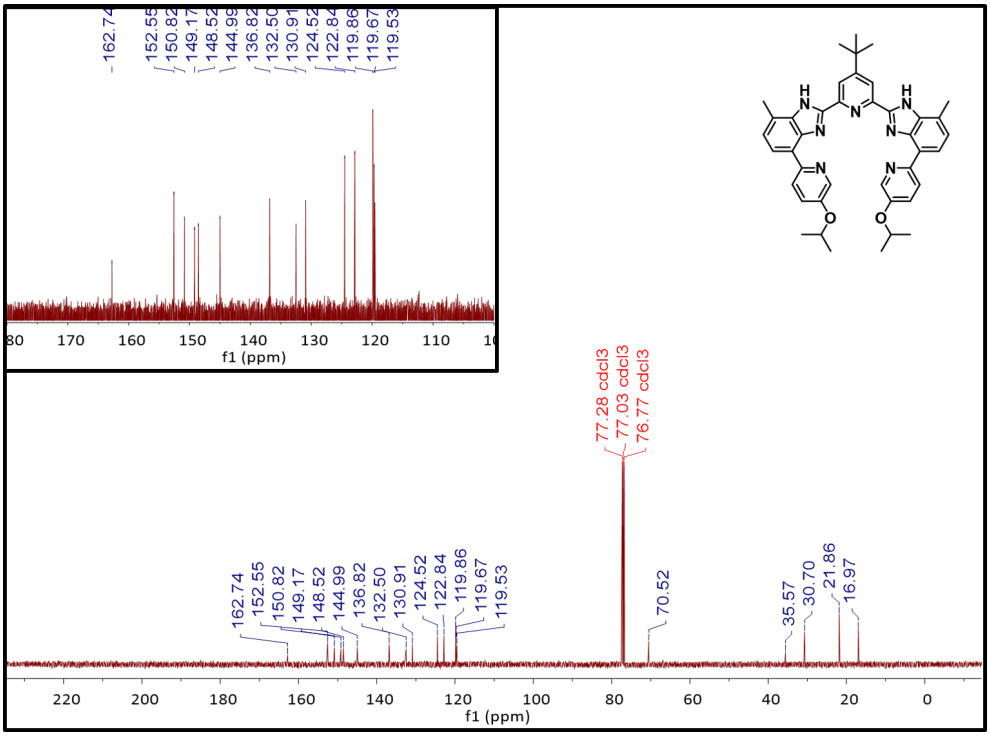

Fig. S26. ^{13}C NMR (125 MHz) spectrum of **L** in $CDCl_3$ (T = 298 K).